nature plants

ARTICLES

PUBLISHED: XX XX 2015 | ARTICLE NUMBER: 15074 | DOI: 10.1038/NPLANTS.2015.74

Chloroplasts play a central role in plant defence and are targeted by pathogen effectors

Marta de Torres-Zabala[1], George Littlejohn[1], Siddharth Jayaraman[1], David Studholme[1], Trevor Bailey[1], Tracy Lawson[2], Michael Tillich[3], Dirk Licht[3], Bettina Bölter[4], Laura Delfino[4], William Truman[5], John Mansfield[6], Nicholas Smirnoff[1] and Murray Grant[1]*

Microbe associated molecular pattern (MAMP) receptors in plants recognize MAMPs and activate basal defences; however a complete understanding of the molecular and physiological mechanisms conferring immunity remains elusive. Pathogens suppress active defence in plants through the combined action of effector proteins. Here we show that the chloroplast is a key component of early immune responses. MAMP perception triggers the rapid, large-scale suppression of nuclear encoded chloroplast-targeted genes (*NECGs*). Virulent *Pseudomonas syringae* effectors reprogramme *NECG* expression in Arabidopsis, target the chloroplast and inhibit photosynthetic CO_2 assimilation through disruption of photosystem II. This activity prevents a chloroplastic reactive oxygen burst. These physiological changes precede bacterial multiplication and coincide with pathogen-induced abscisic acid (ABA) accumulation. MAMP pretreatment protects chloroplasts from effector manipulation, whereas application of ABA or the herbicide DCMU inhibits the MAMP-induced chloroplastic reactive oxygen burst, and enhances growth of a *P. syringae hrpA* mutant that fails to secrete effectors.

Introduction

In plants MAMP-triggered immunity (MTI) provides broad-spectrum protection against a diverse range of potential pathogens. This is achieved through the deployment of a range of surface exposed and cytosolic pattern recognition receptors to detect the presence of potentially pathogenic microbes and activate defence. Successful pathogens attenuate these sophisticated surveillance systems and downstream defences through the collective actions of 'effector' molecules[1,2]. Understanding how the effectors collaborate to cause disease will provide a framework allowing the design of targeted intervention strategies through the rewiring of defence networks to nullify pathogen virulence.

Knowledge of the downstream signalling networks targeted by pathogens, and specifically, the physiological outcomes of these responses, is limited. Chloroplasts play a central role in integrating multiple environmental stimuli[3] and accommodate many biosynthetic pathways, including those for plant hormones. A common strategy deployed by pathogens to hijack host immune signalling is to alter the phytohormone balance. Chloroplasts also produce reactive oxygen species (ROS) that are potentially damaging but which also act as signalling molecules[4] and may have a direct antimicrobial role. Considering the importance of ROS and hormone balance to plant–pathogen interactions[5,6], the chloroplast represents a prime target for manipulation by pathogens.

Understanding the physiological processes targeted by effectors is challenging, not least due to redundancy and cooperativity in pathogen effector repertoires. The hemi-biotroph *Pseudomonas syringae* pv. *tomato* strain DC3000 (DC3000) delivers ~28 type III effector proteins (T3E) into plants via a type III secretion system (T3SS)[7]. To understand the early events underlying DC3000 virulence strategies we analysed high-resolution time course microarray data from leaves challenged with DC3000 or the disarmed *hrpA* mutant, which is unable to produce a functional T3SS.

Results

Focusing on the expression of nuclear encoded chloroplast genes (NECGs; Fig. 1a), our data confirmed previously reported changes in the NECG transcriptome in response to syringe infiltration of both the wild-type and *hrp* mutant bacteria[8], consistent with a conserved plants response to MAMPs. Strikingly, within 2 hpi of bacterial challenge, ~10% of the 3,678 NECGs (comprising ~14% of the genome) were significantly differentially (SD) induced, and between 15% and 20% SD suppressed (as determined using the Bioconductor package LIMMA[9] using the Benjamini–Hochberg false discovery rate correction and 0.05 *P* value cut-off; for summary statistics see Supplementary Table 1). By 4 hpi, NECGs were strongly over-represented, accounting for ~30% of all SD suppressed genes. Notably, transcripts encoding photosynthesis-related processes were suppressed after DC3000 or *hrpA* challenges, whereas some transcripts involved in chorismate, tryptophan and JA biosynthesis were SD induced (Supplementary Fig. 1a). Consistent with the former finding, challenge with the flagellin MAMP peptide, flg22 (ref. 10), or the necrotroph *Botrytis cinerea*[11] also suppresses photosynthesis-related transcripts (Supplementary Fig. 1b). Yet, despite the over-representation of NECGs, clear differences between bacterial challenges were evident 3 hpi (Fig. 1a, DC3000 vs *hrp*) coinciding with the delivery of DC3000 effectors.

The dynamics of SD-regulated NECGs relative to mock challenge are captured by representative scatter plots in Fig. 1b. In these plots red represents NECGs SD regulated between wild-type DC3000 and mock $MgCl_2$ challenge, and blue NECGs SD regulated between *hrpA* mutant and mock. Note that red and blue denote SD-regulated NECGs in response to *hrpA* or wild-type challenge compared to mock but not in both. Green represents NECGs SD changing in both wild-type and *hrpA* challenge, compared with mock inoculation, thus representing MAMP response genes not modified by effectors. To clarify, the differential expression observed represents:

[1]Biosciences, College of Life and Environment Sciences, University of Exeter, Exeter EX4 4QD, UK. [2]School of Biological Sciences, University of Essex, Colchester CO4 3SQ, UK. [3]Max Planck Institute of Molecular Plant Physiology, Am Müehlenberg 1, Potsdam-Golm D-14476, Germany. [4]Department of Biology I, Botany, Ludwig-Maximilians-Universität München, Großhaderner Strase 2–4, Planegg-Martinsried D-82152, Germany. [5]Department of Plant Biology, University of Minnesota, USA. [6]Department of Life Sciences, Imperial College, London, UK. *e-mail: m.r.grant@exeter.ac.uk

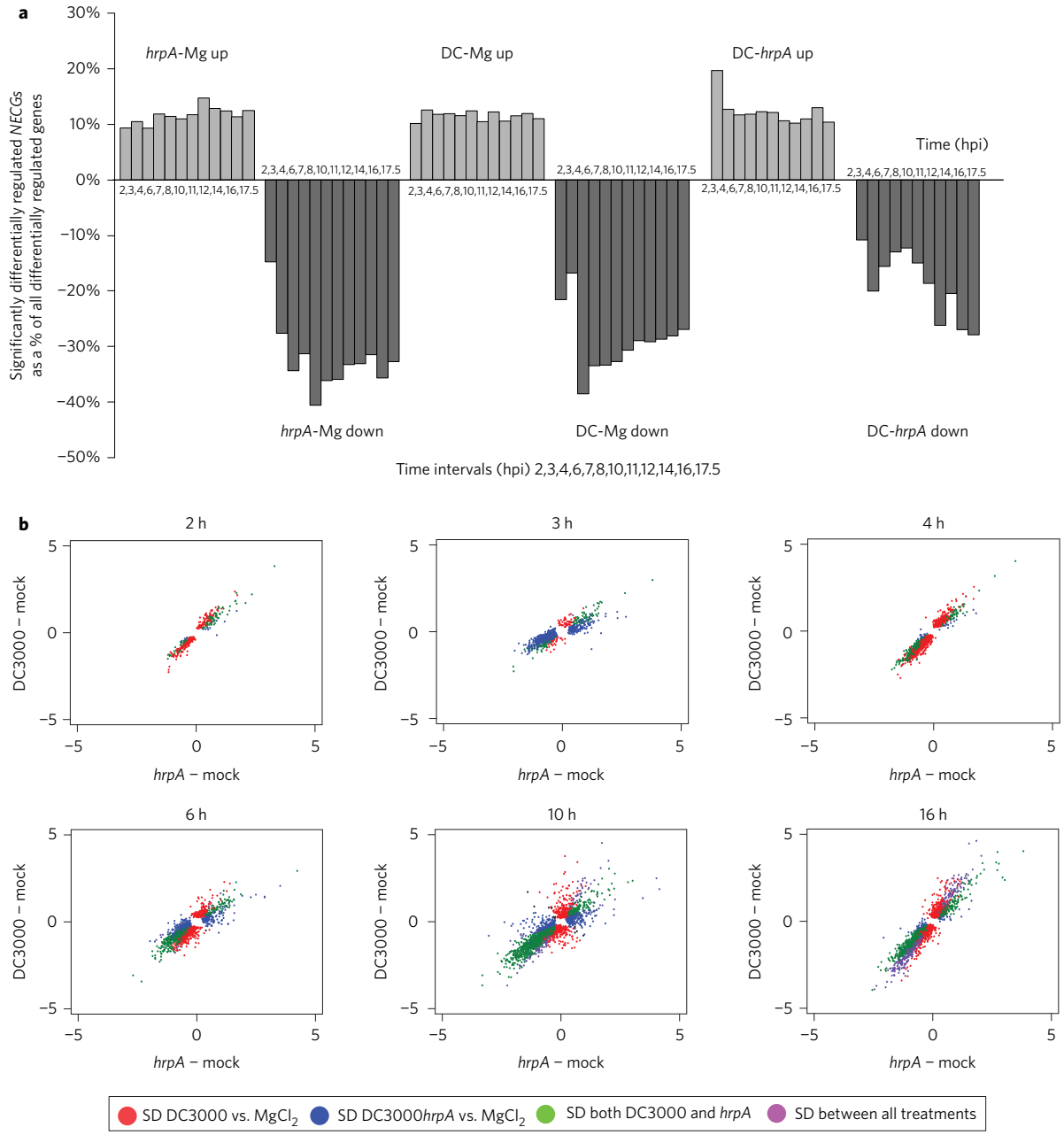

Figure 1 | Nuclear encoded chloroplast transcripts dynamics in defence and disease responses to *Pseudomonas syringae* pv. tomato DC3000. **a**, Representation of significantly up- or downregulated NECGs relative to all SD regulated genes. NECGs represent ~14% of the transcriptome. **b**, Dynamics of NECG expression represented graphically at each time point as a scatter plot. Red represents genes SD in expression between wild-type DC3000 and mock ($MgCl_2$) challenge, and blue SD between *hrpA* mutant and mock. Note that red and blue denote genes SD in response to wild-type or *hrpA* challenges, respectively, but not both. Green describes genes with SD expression in both wild-type and *hrpA* challenges, compared with mock inoculation (MAMP responsive). Violet represents genes SD between all three treatments. The 3,678 NECG annotations were derived from the TAIR9 release. Genes SD expressed between treatments was determined using the Bioconductor package LIMMA using the Benjamini–Hochberg false discovery rate correction and a *P* value cut-off of 0.05.

red, effector induced changes; blue, MAMP modified by effectors; green, persistent MAMP responses and violet, captures NECDs SD regulated between all three treatments (these appear late in the time course).

By 2 hpi a common MAMP response (green) is seen. Already effector modulation of NECGs by DC3000 challenge compared to mock is evident (red profile). However, there are not yet significant differences between DC3000 and *hrpA* treatments (no SD-regulated genes 2 hpi in the DC-*hrpA* analysis, Fig. 1a and Supplementary Table 1). These profiles are capturing the earliest transcriptional reprogramming events resulting from T3E delivery between ~1.5 and 2 hpi (ref. 12), where gene dynamics have not yet diverged from the basal MAMP signature. By 3 hpi, effector activity is clearly evident, with the slope of the plot and the abundant blue signature indicating that T3Es are beginning to override general MAMP responses. The highly dynamic and transient nature of this early transcriptional response is illustrated by a marked change in the NECG signature at 4 hpi, with pronounced red and green profiles. By 6 hpi there is clear impact of T3Es on MAMP regulated genes, reflected by an increasing density and amplitude

of red signals. Genes markedly different between all treatments (violet) increase from a minor component 6 hpi to represent a major proportion of SD genes 16 hpi. Notably, MAMP-induced responses (green) are still abundant 16 hpi, reinforcing continuous transcriptional regulation of NECGs throughout the expression of defence. In summary, NECGs are highly represented amongst SD expressed genes between mock and either *hrpA* mutant or virulent wild-type DC3000. Effectors modify the MAMP signature as early as 2 hpi, with NECGs SD regulated by T3Es measurable within 3 hpi. Effectors act to both enhance and suppress gene expression caused by MAMPs and impose a transcriptome representing successful establishment of disease, a large proportion of which comprises NECGs (Supplementary Table 1 and Fig. 1a).

The strong and early suppression of photosynthesis-related transcripts after both challenges is consistent with photosynthetic processes being targeted by MAMPs (Supplementary Fig. 1). To explore the physiological impacts of the observed dynamic changes in NECG expression we recorded net photosynthetic CO_2 assimilation (A_{sat}) following inoculation. Strikingly, DC3000 but not *hrpA* challenged leaves showed a decrease in assimilation between 6 and 8 hpi (Fig. 2a). Unexpectedly, A/C_i curves (reporting photosynthesis versus intercellular CO_2) showed that photosynthesis is not restored by high intercellular CO_2 (Fig. 2b). Thus stomatal closure would not simply explain the DC3000-induced suppression of CO_2 assimilation. The rapid suppression of photosynthesis represents one of the earliest physiological responses detected to DC3000. We used chlorophyll fluorescence imaging to further investigate the mechanism of DC3000 action. Challenge with DC3000 but not *hrpA* or mock inoculation caused a rapid decrease in maximum dark-adapted quantum efficiency (*Fv*/*Fm*; Fig. 2c,i), maximum operating efficiency of photosystem II (PSII) photochemistry at a given light intensity if all the PSII centres are oxidized (*Fv*′/*Fm*′, Fig. 2d) and the efficiency with which light absorbed by PSII is used for Q_A reduction and linear electron transport at a given light intensity (*Fq*′/*Fm*′; Fig. 2e). qL also increased by 6 hpi with DC3000 but not *hrpA* (Fig. 2f). qL estimates the fraction of open PSII centres and the oxidation state of the primary PSII quinone acceptor (Q_A, ref. 13), indicating that the Q_A is more oxidized and suggesting decreased electron transport from PSII. Non-photochemical quenching (NPQ) increased transiently at 4–10 hpi (Fig. 2g,i). Elevated NPQ indicates increased excitation energy dissipation as heat, caused either by proton gradient-dependent processes involving PsbS and xanthophylls (energy-dependent quenching), or photoinhibitory quenching[14].

Inhibition of photosynthesis by a biotrophic pathogen is potentially counter-intuitive, because it would reduce sugars available to the pathogen. We verified the effect by recording $^{14}CO_2$ assimilation. After 10 h, leaves inoculated with DC3000 fixed less $^{14}CO_2$ than mock or *hrpA*-inoculated leaves (Supplementary Fig. 2a) whereas the neighbouring uninoculated leaves were unaffected (Supplementary Fig. 2b). DC3000 would not lack fixed ^{14}C presumably because it would be translocated from the neighbouring leaves, thereby providing carbon sources for the pathogen.

Our data are consistent with rapid T3E inactivation of PSII, resulting in decreased electron transport and non-stomatal inhibition of CO_2 assimilation. While decreases in transcript abundance of *NECG*s have been observed[8,11,15,16], they have not previously been linked to changes in photosynthetic metabolism. Critically, the T3E-induced changes in chloroplast physiology are initiated prior to rapid bacterial multiplication which occurs only after a period of 6–8 h of bacteriostasis in the intercellular space, during which the dynamic exchange of MAMP signals and effectors takes place (Fig. 2h)[17]. T3E inactivation of PSII is not specific to DC3000, both *Ps* pv. *maculicola* M4 (ref. 18) and *Xanthomonas campestris* pv. *campestris* (Xcc) race 6 (ref. 19) also suppressed *Fv*/*Fm*, but this effect occurred later and was weaker, correlating with their reduced virulence in *Arabidopsis* (Supplementary Fig. 3).

We further explored the surprising finding that, despite suppressing a significant proportion of NECGs (Supplementary Table 1 and Fig. 1) photosynthesis was unaffected in *hrpA* challenged leaves (Fig. 2a). Remarkably, DC3000 suppression of *Fv*/*Fm* was prevented in leaves pretreated 24 h previously with flg22 (1 μM) but not SA (1 mM) (Fig. 3a and Supplementary Fig. 4a). Non-pathogenic *P. fluorescens* did not affect *Fv*/*Fm* and CUCPB6032 (ref. 20), a reduced virulence DC3000 strain, had less effect on *Fv*/*Fm* than DC3000 (Fig. 3b and Supplementary Fig. 4b). By contrast, the *fliC* mutant, which lacks bacterial flagellin[21], elicited a much stronger reduction in *Fv*/*Fm* compared to DC3000, indicating that flagellin perception plays an important role in the maintenance of photosynthetic capability (Fig. 3b and Supplementary Fig. 4b). Pretreatment of the MAMP receptor mutant *fls2*-2 (ref. 22) with flg22 failed to prevent DC3000 suppression of *Fv*/*Fm*, whereas activation of the bacterial elongation factor thermo unstable (EF-Tu) receptor by elf18 MAMP peptide[23] protects the chloroplast in the *fls2* background (Fig. 3c and Supplementary Fig. 4c). Correspondingly, the hypersusceptible *eds1* mutant, which compromises MAMP and effector triggered immunity[24] displayed markedly enhanced suppression of *Fv*/*Fm* (Supplementary Fig. 4d). The protection of the chloroplast from effector-mediated perturbations has emerged as an important and unexpected component of MTI.

Effectors delivered by DC3000 induce rapid increases in ABA within 6 hpi and pretreatment with ABA enhances susceptibility to DC3000 (ref. 17). It was therefore important to determine whether ABA homeostasis influenced photosynthesis. Co-infiltration of DC3000 with ABA increased NPQ (Supplementary Fig. 4e) and decreased *Fv*/*Fm* (Fig. 3d and Supplementary Fig. 5a) compared with DC3000 alone. Importantly, neither ABA alone nor co-infiltration with *hrpA* affected *Fv*/*Fm*. ABA pretreatment also induced larger decreases in *Fv*/*Fm* following challenge with *Psm*M4, or two virulent races of *Xcc* (Fig. 3e and Supplementary Fig. 5b). *Arabidopsis* ABA hypersensitive protein phosphatase 2C (PP2C) mutants are more susceptible to DC3000 (ref. 25) whereas the ABA deficient *Arabidopsis aldehyde oxidase 3* (*aao3*) mutant is more resistant to DC3000 infection[17]. DC3000 challenged PP2C triple mutant *abi1/abi2/hab1* (*triple*)[26] showed significantly faster and stronger suppression of *Fv*/*Fm* compared to Col-0, whereas *Fv*/*Fm* in the *aao3* mutant was less affected by DC3000 challenge compared to wild-type Col-0 (Supplementary Fig. 5d). Therefore effector perception rapidly modifies ABA signalling, which directly impacts on photosynthesis during the critical first few hours after bacterial challenge.

To link chlorophyll fluorescence dynamics with suppression of basal defence we first monitored luciferase activity of a transgenic line expressing *FLS2 induced receptor kinase 1* (*FRK1*)[27] fused to luciferase (Fig. 3g). The construct reports activation of FLS2. The suppression of luciferase activity between 2 and 4 hpi DC3000 was found to correlate with specific changes in NECG expression (Fig. 1) and is coincident with suppression of photosynthesis (Fig. 2). Notably, all these transcriptional changes occur before rapid bacterial multiplication 8 hpi. Secondly we found that the hypersensitive *triple* PP2C mutant showed strikingly rapid suppression of *Fv*/*Fm*, which was phenocopied by exogenous application of 10 μM ABA, whereas *Fv*/*Fm* was only mildly reduced in DC3000 challenged *aao3* leaves (Fig. 3g). In summary, Fig. 3a–c links *Fv*/*Fm* to suppression of MTI, showing that flg22 but, surprisingly, not SA (which is not synthesized until significantly later in the infection process[17]) prevents T3E suppression of *Fv*/*Fm* whereas *fliC* mutant challenge enhanced *Fv*/*Fm* suppression. Figure 3d–f illustrates the importance of pathogen-induced ABA in suppression of *Fv*/*Fm*. These panels show that (i) effectors have to be delivered and that (ii) virulent bacteria produce ABA to suppress *Fv*/*Fm*

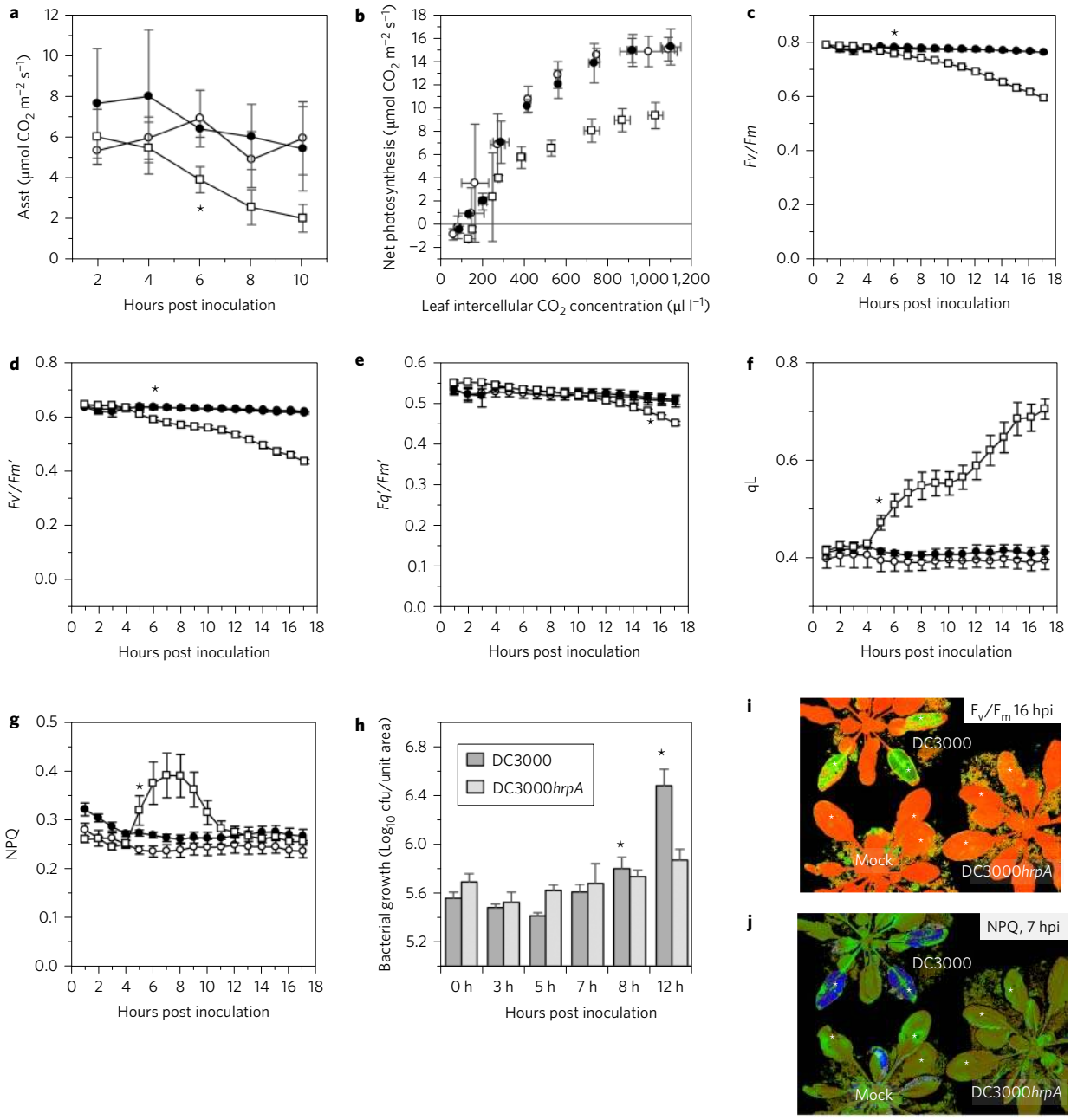

Figure 2 | *Pseudomonas syringae* DC3000 rapidly inhibits photosynthesis in *Arabidopsis thaliana*. For all panels, mock – open circle, DC3000*hrpA* – closed circles, DC3000 – open squares. **a**, DC3000 decreases photosynthetic CO_2 assimilation in saturating light (A_{sat}). **b**, A/C_i curve showing the relationship between photosynthesis (A) and intercellular CO_2 concentration (C_i) at 10 hpi. **c**, Maximum quantum efficiency of PSII (*Fv/Fm*), **d**, maximum light adapted quantum efficiency of PSII (*Fv′/Fm′*) and **e**, PSII operating efficiency (*Fq′/Fm′*) are decreased by DC3000 challenge and **f**, photochemical quenching of PSII (qL) is increased. **g**, NPQ transiently increases 4 hpi after DC3000 inoculation. **h**, DC3000 bacterial growth (inoculum of ~0.5×10^8 cfu ml^{-1}) is restricted until 8 hpi. Asterisks show significant differences in bacterial growth (*t*-test, $P < 0.05$) from time 0 (mean ± SD; $n = 6$). **i**, False colour image of *Fv/Fm* at 16 hpi showing a decrease (green/yellow) after DC3000 challenge. Asterisks show inoculated leaves. **j**, False colour image of NPQ at 7 hpi showing the increase (blue) after DC3000 challenge. Asterisks show inoculated leaves. Photosynthesis values (**a**) are means ± SD ($n = 4$), and show that DC3000 differs significantly from DC3000*hrpA* and mock treatments from 8 hpi (*$P < 0.001$; two-way ANOVA). Chlorophyll fluorescence parameters (**c**–**g**) are means ± SD (mock and *hrpA*, $n = 3$; DC3000, $n = 4$). ANOVA with the least significant difference *post hoc* test and Bonferroni multiple comparison correction shows that DC3000 differs significantly from DC3000*hrpA* and mock treatments for all time points at and beyond the asterisk ($P < 0.05$).

prior to bacterial multiplication. Additionally, Fig. 3f provides the temporal context, linking suppression of basal immunity to reduced *Fv/Fm* and the important role of pathogen-induced ABA in this process. We conclude that inhibition of photosynthesis is a prerequisite for suppression of MTI leading to bacterial multiplication (Fig. 1j) and that these effects are underpinned by modulation of ABA signalling.

Effectors induce transcriptional changes in NECGs but the rapid suppression of NPQ and *Fv/Fm* also suggested the possibility of their direct action in the chloroplast. The *P. syringae* effectors, HopI1, HopN1 and AvrRps4/HopK, have been localized to the chloroplast[28–32]. Notably, AvrRps4 and HopK use non-canonical import sequences[30] suggesting effectors have evolved multiple strategies to localize to chloroplasts. HopN1, a cysteine protease,

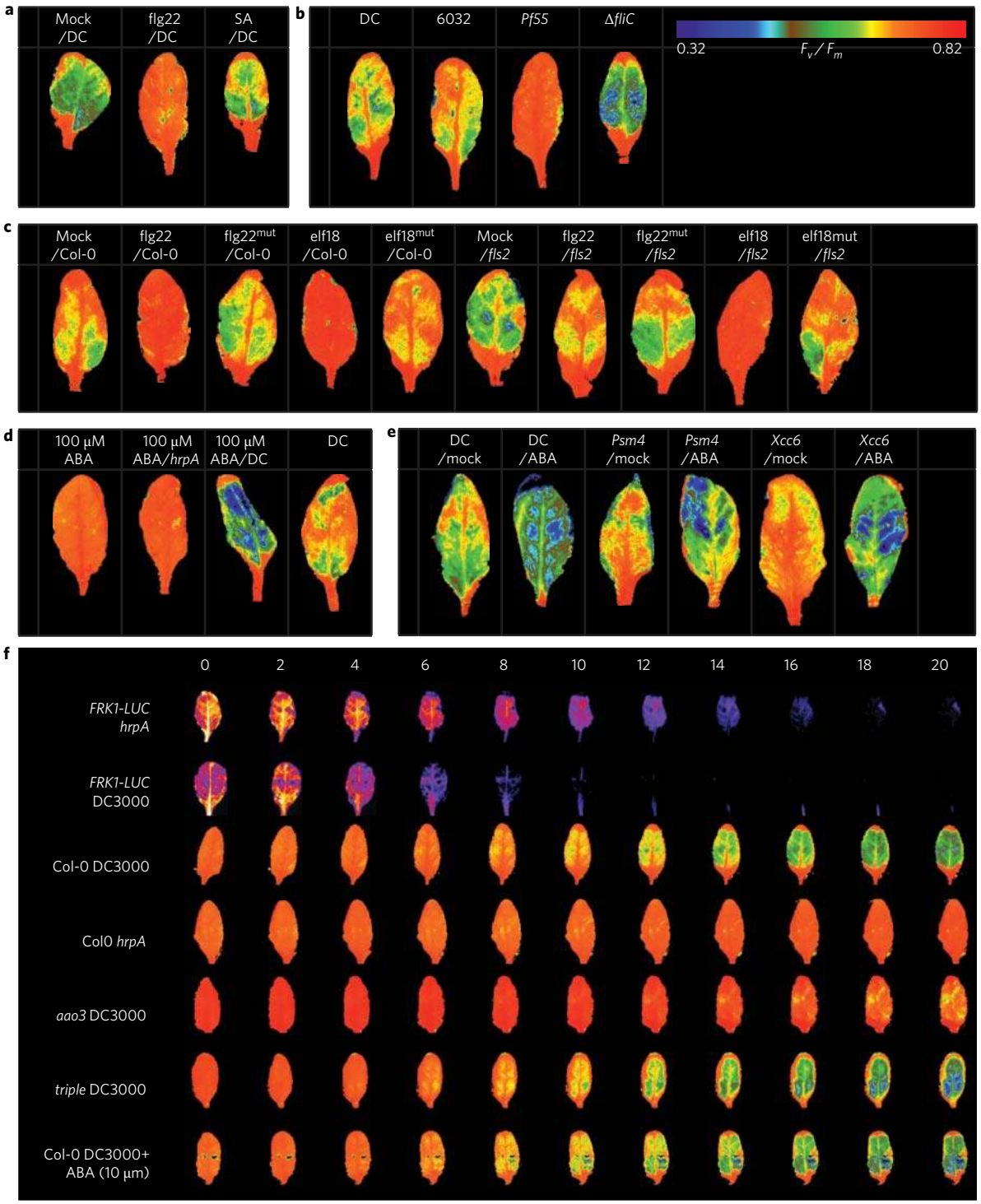

Figure 3 | DC3000 effectors suppress *Fv/Fm*, in an ABA dependent manner. a–e *Fv/Fm* in single leaves of representative treatments at 18 hpi, and **f**, representative leaves across a treatment time course. See Supplementary Figs 4 and 5 for quantitative data and whole plant images. MAMP pretreatment attenuates *P. syringae* suppression of *Fv/Fm*. **a**, Pretreatment 24 hpi with flagellin peptide (flg22; 1 µM) but not SA (1 mM), prevents DC3000 suppression of *Fv/Fm*. **b**, MAMPs restrict T3E mediated *Fv/Fm* suppression. Representative Col-0 leaves challenged with non-pathogenic *Pseudomonas fluorescens* (Pf55) containing a functional T3SS, CUCPB6032 a minimally virulent DC3000 derivative, DC3000 or Δ*fliC* which lacks bacterial flagella[20,21]. A strong reduction in *Fv/Fm* (18 hpi) elicited by the *fliC* mutant reflects the importance of MAMPs in chloroplast mediated MTI. **c**, Col-0 or *fls2-2* mutant leaves mock treated or challenged with flg22, elf18, or their respective mutant non-binding ligands, flg22-tu or elf18^{mut} (all at 1 µM). After 24 h, leaves were challenged with DC3000. **d**, T3E suppression of *Fv/Fm* is enhanced by ABA. Col-0 leaves challenged with ABA alone, or co-infiltrated with either *hrpA* or DC3000 at 100 µM (see Supplementary Fig. 4e (NPQ) and 5a (*Fv/Fm*) for additional concentrations). **e**, ABA enhances suppression of *Fv/Fm* by *P. maculicola* M4 (*Psm4*) or *X. campestris* pv. *campestris* (*Xcc*) race 6 (see Supplementary Fig. 5B for *Xcc* race 1). **f**, Summary of *Fv/Fm* responses. Hourly measurements of *Fv/Fm* in DC3000 challenged leaves of wild-type (Col-0), the hypersensitive *triple* and ABA deficient *aao3* mutants or following co-infiltration with ABA (10 µM) compared DC3000*hrpA* challenge (see Supplementary Fig. 5c for additional ABA mutant data). A reporter line expressing *flagellin induced receptor kinase 1* (*FRK1*) fused to luciferase was used to monitor suppression of basal defence by DC3000. All bacterial treatments were at ~0.5×10^8 S ml^{-1}.

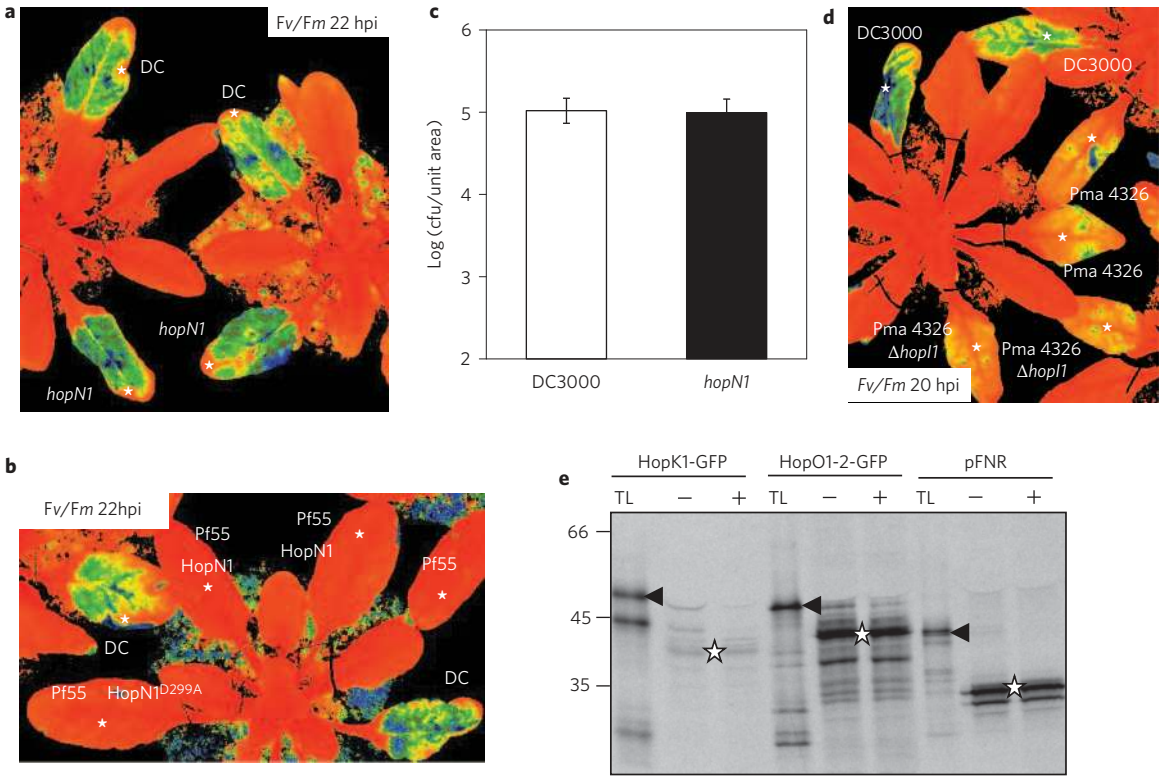

Figure 4 | Chloroplast localized HopN1 and HopI1 do not modify *Fv/Fm*. **a**,**b**, Neither deletion of HopN1 nor delivery of HopN1, or its catalytic derivative HopN1^{D229A}, modified *Fv/Fm*. **c**, Deletion of HopN1 does not affect susceptibility to DC3000. Bacterial growth in *hopN1* 4 dpi with DC3000 (~0.5×10^5 cfu ml^{-1}; mean, $n = 6$, error SD ± 1). **d**, Deletion of HopI1 does not impact *Fv/Fm*. **e**, The N-terminus of HopO1-2 is imported into chloroplasts. The import of effector N-termini (~150 aa fused to GFP) into pea chloroplasts was analysed using *in vitro* transcription/translation assays and visualized by $^{35}S^{-}$autoradiography. The previously validated HopK (control effector), the putative effector ribosyltransferase, HopO1-2 and an import control (pFNR; precursor of the chloroplast-targeted ferredoxin-NADP(+) oxidoreductase) were transported into isolated pea chloroplasts. Their putative mature forms (labelled by asterisks) but not their precursors (arrowheads) are resistant to thermolysin treatment. TL: 10% of translation product used for import experiments, ±: import reactions with and without thermolysin treatment.

specifically targets and proteolytically cleaves tomato PsbQ (ref. 31), an extrinsic protein of PSII. In *Nicotiana benthamiana* HopN1 reduced early immunity responses, altered electron transport and suppressed ROS production[31]. However, we found that neither DC3000Δ*HopN1* nor delivery of HopN1 or its catalytically inactive HopN1^{D299A} derivative by *P. fluorescens* altered *Fv/Fm* or reduced virulence on *Arabidopsis* (Fig. 4a–c). Similarly HopI1, which modifies thylakoid structure, suppresses salicylic acid accumulation and targets HSP70, did not alter *Fv/Fm* (Fig. 4d)[32]. These data suggest multiple effectors may cooperate to alter PSII function.

To explore organelle targeting more fully, we analysed a core set of 48 *Pseudomonas* effector proteins (derived from www.effector.org) with ChloroP (ref. 33) and identified 21 possible chloroplast-targeted effectors, including the experimentally validated HopK1 and HopN1 (Supplementary Table 2). Using serine frequency scanning to compare the 28 effectors with known plant chloroplast localized proteins confirmed a potential chloroplast location for 21 of the effectors (Supplementary Fig. 6). ChloroP predicted potential chloroplast targeting sequences in putative effectors from a range of other sequenced bacterial genomes, including 54% of the 28 DC3000 effectors and 53% of the 19 *Xcc* effectors (Supplementary Table 3). Further evidence that effectors target the chloroplast was derived from the yeast two hybrid interaction data of plant pathogen effectors against ~8,000 *Arabidopsis* proteins[34]. An interaction network generated for *P. syringae* effectors predicted a number of T3Es (e.g. HopR1, HopBB1, HopZ) that can interact with multiple chloroplast proteins. These chloroplast predicted proteins themselves interact with two or more effectors (Supplementary Fig. 7a). Thus sequence unrelated effectors are potentially chloroplast localized and have common potential susceptibility targets, consistent with redundancy and robustness in virulence strategies.

Based on these data we tested whether the N-termini (~150 aa) of a set of the putatively chloroplast localized effectors are imported in chloroplast import assays[35]. We chose HopR1 because it is a widely distributed T3E in proteobacterial phytopathogens[36], and HopO1-2 because it has predicted ADP-ribosyl-transferase activity, similar to HopU1, that ribosylates at least three chloroplast RNA-binding proteins *in vitro*, although there is no evidence that HopU1 localizes to the chloroplast[37]. We found that *in vitro* translated HopO1-2 was efficiently imported into isolated pea chloroplasts (Fig. 4e). HopO1-2 is predicted to interact with one plastid localized protein (At3g07780). HopR1 was also imported into chloroplasts (Supplementary Fig. 7b,c). Four independent effectors are predicted to interact with one or more of HopR1's targets, and AvrPto and HopBB1 share HopR1's chloroplast targets (Supplementary Fig. 7a). Notably, the chloroplast target of HopR1 (and HopBB1), PTF1/TCP13 (PLASTID TRANSCRIPTION FACTOR 1/TEOSINTE BRANCHED1, CYCLOIDEA AND PCF TRANSCRIPTION FACTOR 13) is a transcription factor that binds to the promoter of *psbD* (ref. 38). *psbD* encodes the PSII reaction centre protein D2, which along with D1 (PsbA) bind all the redox-active cofactors involved in the energy conversion process[39]. Loss of D2 blocks electron transport, resulting in destabilization of the PSII complex[40]. TCP13 loss of function plants are more resistant to DC3000 but more susceptible to *Golovinomyces orontii* and *Hyaloperonospora arabidopsidis*[41].

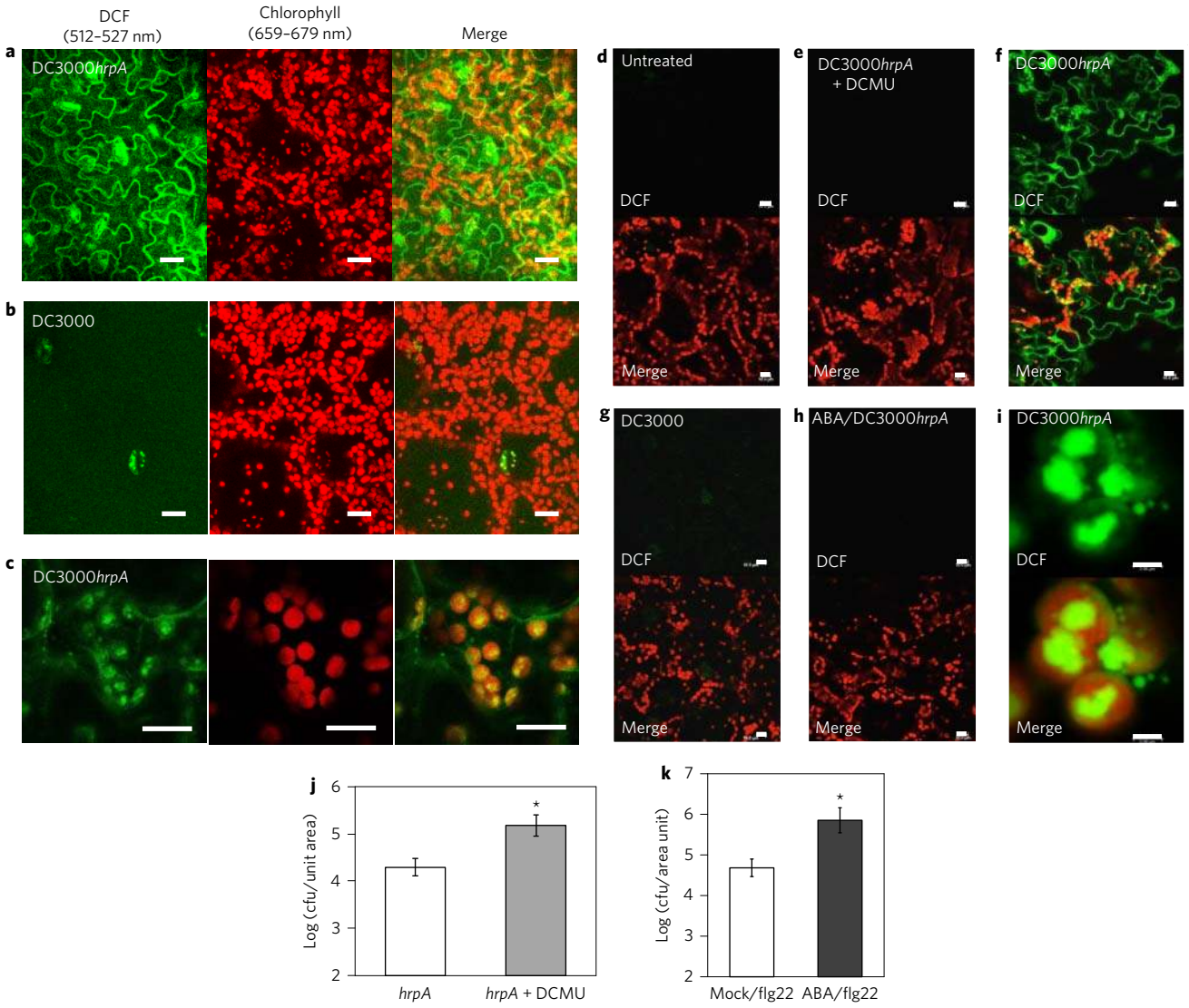

Figure 5 | Effectors suppression of a photosynthesis-derived reactive species burst is necessary to overcome basal defences and promote pathogen growth. The conversion of 2′7′-dichlorodihydrofluorescein diacetate to dichlorofluorescein (DCF) was used to monitor reactive species generation in **a**,**c**,**f**,**i**, DC3000*hrpA*, **b**,**g**, DC3000 or **d**, mock challenged leaves by confocal microscopy and images merged with chlorophyll emission. Inhibiting electron transport from PSII with the herbicide DCMU (10 μM) (**e**) or prior application of ABA (**h**), both block the DC3000*hrpA* reactive species burst. All scale bars 10 μm, except final panel (2 μm). All bacterial challenges (**a**–**i**) were at ~0.5×10^8 cfu ml^{-1} and images captured between 5 and 5:40 hpi. **j**, Co-infiltration of DCMU (10 μM) with DC3000*hrpA* (~1×10^6 cfu ml^{-1}) led to enhanced bacterial multiplication. **k**, Pretreatment with ABA prevents flg22 induced resistance to DC3000. Leaves were either mock or ABA (10 μM) pretreated then 24 h later inoculated with flg22 (1 μM). Leaves were challenged 24 h later with DC3000 (~0.5×10^5 cfu ml^{-1}) and bacterial growth measured 3 dpi (means $n = 6$, ± SD), asterisk indicates significant differences between treatments ($P < 0.05$, Student's *t*-test).

The generation of apoplastic ROS is a hallmark of MTI[42]. Photosynthesis is also a potential source of ROS in basal defence. We hypothesized that suppression of photosynthesis-derived ROS may be a specific mechanism to attenuate basal defence. We examined ROS production after apoplastic ROS generation[43] and prior to bacterial multiplication using the probe 2′7′-dichlorodihydrofluorescein diacetate (H_2DCF-DA, ref. 44). Strikingly, by 5 hpi, a strong increase in oxidized dichlorofluorescein (DCF) signal was detected by confocal microscopy in *hrpA* (Fig. 5a,c,f,i) but not DC3000 challenged leaf cells (Fig. 5b,g) or mock inoculated tissue (Fig. 5d). Although the probe is diffusible after hydrolysis or oxidation, a strong oxidized DCF signal was clearly seen in individual chloroplasts (Fig. 5c,i). H_2DCF-DA is sensitive to H_2O_2 but is not specific[45]. Blocking electron transport from PSII with 3-(3,4-dichlorophenyl)-1,1-dimethylurea (DCMU) has previously been shown to inhibit the production of H_2O_2 by oxygen photoreduction at PSI[46] and to increase singlet oxygen production by PSII[47]. DCMU co-infiltration (10 μM) abolished the *hrpA*-induced probe oxidation, consistent with photosynthetic production of H_2O_2 or another oxidant derived from it (Fig. 5e). We conclude that the effector-dependent inhibition of photosynthetic electron transport decreases MAMP-induced photosynthetic hydrogen peroxide production. To explore the link between photosynthetic ROS production and bacterial growth we co-infiltrated Arabidopsis leaves with *hrpA* and DCMU. Remarkably, DCMU treatment not only abolished the induction of ROS by *hrpA* challenge (Fig. 5j), but also significantly enhanced growth of *hrpA*, suggesting that inhibition of photosynthesis and consequent restriction of chloroplast-sourced ROS production is required for full immunity (Fig. 5d). ABA pretreatment enhances growth of *hrpA* (ref. 25).

Consistently, ABA pretreatment prior to *hrpA* challenge also abolished ROS production (Fig. 5h) and ABA pretreatment of leaves 24 h prior to flg22 treatment also prevented flg22-mediated restriction of DC3000 growth (Fig. 5k).

PSII disruption is also associated with singlet oxygen production[48]. Publically available microarray data revealed that the DC3000 NECG signature was remarkably similar to those resulting from treatments (lincomycin, norflurazon) and mutants (*flu1*) which cause singlet oxygen formation (Supplementary Fig. 8). However, these sampling times are considerably later than the chloroplast ROS generation and coincide with exponential bacterial growth. As neither *executer* single or double mutant suppressors of *flu1* (*ex1/ex2,* ref. 49) showed altered susceptibility to DC3000 (Supplementary Fig. 9a) we conclude that these signatures are a late response to infection. Moreover, the classical *genome uncoupled* mutants[50] *gun4*, *gun5/abar-2* (which are largely responsible for the singlet oxygen signature in Supplementary Fig. 8) and *gun1*, all exhibited wild-type susceptibility (Supplementary Fig. 9b,c). Thus a different mechanism of inter-organellar signalling appears to be responsible for the MAMP and effector associated transcriptional repression of NECGs.

Discussion

We provide new insights into mechanisms underpinning plant innate immunity and phytobacterial virulence strategies. Using virulent DC3000 and a T3SS deficient DC3000*hrpA* mutant we were able to examine initial events in MTI and suppression of MTI. We show that the chloroplast plays an early and important central role in integrating disease and defence signals. MAMP recognition leads to rapid transcriptional reprogramming of chloroplast encoded transcripts. Within 3 hpi, virulent DC3000 bacteria modify the NECG transcripts and deliver a subset of effectors into the chloroplast. Thus the DC3000 virulence strategy acts both transcriptionally and post-transcriptionally to target the chloroplast, resulting in a rapid, non-stomatal inhibition of photosynthesis in a T3E-dependent manner. Chloroplast-targeted effectors collaborate to destabilize PSII and consequent inhibition of photosynthetic electron transport decreases the MAMP-induced ROS production we observed 5–6 hpi. Pathogen-induced ABA contributes significantly to suppression of immunity. PSII suppression can be mimicked by exogenous application of ABA, or attenuated by prior activation of innate immune receptors by MAMPs. Rational engineering of intervention strategies to protect chloroplasts from bacterial effectors may well provide a novel approach to broad-spectrum resistance against bacterial pathogens. If, as seems probable, key non-bacterial crop pathogens adopt similar virulence strategies, then chloroplast intervention provides considerable scope for restricting crop losses and simultaneously improving productivity.

Methods

Arabidopsis growth conditions. *Arabidopsis thaliana* wild-type and mutant seed were sown in a sieved compost mix (Levingston's F2 compost + sand (LEV206): vermiculite (medium grade) mixed in a 6:1 ratio). Plants were grown in a controlled environment growth chamber under a 10 h day (23 °C; 120 μmol m^{-2} s^{-1}) and 14 h night (20 °C) regime with relative humidity set to 65%. Plants were grown for 4–5 weeks prior to use.

Bacterial growth, maintenance and inoculation. *Pseudomonas syringae* strains were grown on solidified Kings B media containing appropriate antibiotics as described[8]. *Xanthomonas campestris* strains were grown on Kings B without antibiotics. For inoculation, overnight cultures were grown with shaking (200 rpm) at 28 °C. Cells were harvested (2,000 g × 8 min), washed and resuspended in 10 mM $MgCl_2$. Cell density was adjusted to OD_{600} 0.15 (~0.75×10^8 colony forming units (cfu) ml^{-1}) for fluorescence and luciferase imaging or high inoculum growth curves, or OD_{600} 0.0002 for low inoculum growth assays. All growth curves were repeated at least twice. All fluorescence and luciferase imaging experiments were performed at least four times.

Microarray data. RNA was extracted at the appropriate time point from a single challenged day 8 leaf and samples were cleaned up using a Qiagen RNeasy Plant mini kit according to the manufacturer's instructions. Samples were hybridized to CATMA arrays[51] and data processed exactly as described[52]. Data comprise means from four single leaf biological replicates and two technical replicates per time point and are deposited at GEO (Gene Expression Omnibus) under the accession number *GSE56094*. The 32,578 CATMA probes were mapped to 25,115 unique AGI identifiers using the TAIR 9 release. The NECGs were derived as follows: the TAIR GO.Slim annotations for 'Chloroplast' (accessed 19 February 2013) were used to identify 3,678 genes represented by the CATMA probes. NECG expression data for Fig. 1 were generated using the Bioconductor package LIMMA (Linear Models for Microarray Data) applying a *P* value cut-off of 0.05 and FDR correction using the Benjamini–Hochberg method and annotations derived from the TAIR9 release.

Chlorophyll fluorescence imaging. Photosystem II chlorophyll fluorescence imaging of Arabidopsis rosettes was performed with a CF Imager (Technologica Ltd, Colchester, UK). Plants were placed in the chamber for 40 min post-inoculation and then dark adapted for 20 min. This was followed by a saturating light pulse (6,349 μmol m^{-2} s^{-1} for 0.8 s) to maximum obtain dark-adapted fluorescence (*Fm*). Actinic light (120 μmol m^{-2} s^{-1} – the same as plant growth light intensity) was then applied for 15 min, followed by a saturating pulse to obtain maximum light adapted fluorescence (*Fm′*). The plants were then left for a further 24 min in actinic light before returning to the dark for 20 min. At this point the cycle of measurements (59 min duration) was repeated 23 times. *Fm*, *Fm′* and *Fo* (minimal fluorescence with fully oxidized PSII centres) were used to calculate chlorophyll fluorescence parameters related to photosystem II photochemistry: *Fv*/*Fm* (maximum dark-adapted quantum efficiency); maximum light adapted quantum efficiency (*Fv′*/*Fm′*); operating quantum efficiency (*Fq′*/*Fm′*); fraction of open PSII centres (qL) and NPQ. The values were calculated as described by Baker[13]. The temperature during measurements was 20 °C.

Photosynthetic measurements. Photosynthetic gas exchange measurements were made using a portable open gas analysis system (CIRAS1, PP Systems, Amesbury, Massachusetts, USA). The analyser was calibrated before use for CO_2, using a standard gas (±2.5% tolerance) (BOC, UK) and for H_2O using a dew point generator (LI-610, Li-Cor). The response of assimilation (*A*) rate to intercellular CO_2 concentration (C_i) was measured on whole leaves at a saturating photosynthetic photon flux density (PPFD) of ~600 μmol m^{-2} s^{-1}. Leaves were initially stabilized in the cuvette at ambient CO_2 concentration (Ca) of 400 μmol mol^{-1}, leaf temperature was maintained at 23 ± 2 °C and vapour pressure deficit was ~1 kPa. Following stabilization C_a was decreased to 300, 200, 100 and 75 μmol mol^{-1} before returning to the initial concentration. This was followed by an increase to 550, 700, 1,000 and 1,200 μmol mol^{-1}. Readings were recorded when CO_2 assimilation (*A*) had stabilized to the new C_a conditions (after about 2 min). The maximum velocity of Rubisco for carboxylation (V_{cmax}), the maximum rate of electron transport demand for RuBP regeneration (J_{max}), and respiration rate (R_d) were derived by curve fitting as described[53].

The response of assimilation (*A*) rate to changing PPFD was measured using the same open system immediately following the A/C_i curves described above. Leaves were initially stabilized at saturating irradiance (~600 μmol m^{-2} s^{-1}) and current ambient CO_2 concentration (400 μmol m^{-2} s^{-1}), after which PPFD was reduced in a stepwise manner to 0 μmol m^{-2} s^{-1}. Readings were recorded when CO_2 assimilation (*A*) had stabilized to the new PPFD levels (after about 1 min). The quantum efficiency was determined from the linear slope of the curve at low PPFDs (between 0 and 100 μmol m^{-2} s^{-1}), while A_{sat} was determined as the maximum light saturated rate of *A*.

Confocal microscopy. Plants were challenged as described above. Following treatment (2–3 hpi), leaves were detached and floated, adaxial surface upwards, in a solution of 10 mM $MgCl_2$ containing 10 μM 2′7′-dichlorodihydrofluorescein diacetate (H_2DCF-DA; Enzo) for at least 1 h, then washed for 20 min before imaging. Pretreatment with ABA was as described[17]. DCMU (**3**-(3,4-dichlorophenyl)-1,1-dimethylurea; Sigma) was co-infiltrated with bacteria at a concentration of 10 μM. Samples were mounted in perfluorodecalin[54] and images were captured on a Leica SP8 using a 40× oil immersion lens. Argon laser excitation at 488 nm and an emission window of 512–527 nm was used to capture the dichlorofluorescein (DCF) signal. Chloroplast fluorescence was measured at 659–679 nm.

***In vivo* chemiluminescence imaging.** *FRK1-LUC* plants (4–5 weeks old) were sprayed with 1 mM D-luciferin (Sigma) in 0.01% w/v Triton X-100 and incubated in the dark for 30 min. Sprayed plants were treated accordingly, placed in a dark box and luciferase images acquired in a dark box at room temperature using a Hamamatsu ORCAII ER CCD camera with a 35 mm f2.8 Nikkor lens. Photons were counted every 5 min at 2 × 2 binning mode using Wasabi imaging software (Hamamatsu Photonics).

Exploring common suppression patterns of NECGs in publically available microarray datasets. Affymetrix gene chip data was obtained from NCBI GEO (http://www.ncbi.nlm.nih.gov/geo/) or from NASCARRAYS (http://affymetrix.arabidopsis.info) for the following experiments: NASCARRAYS59, NASCARRAYS120, NASCARRAYS414, GSE10876, GSE49596, GSE10812,

GSE5726, GSE12887 and GSE5770. RMA normalization was performed using the Bioconductor package affy; replicates were averaged and the $\log_2$ ratios were calculated between treatment and mock or wild-type and mutant. Transcript data was available for 3,445 NECG probe sets, these were filtered to 2,676 probe sets which exhibited expression changes greater than 1.5 fold in at least one treatment. Complete linkage hierarchical clustering was carried out using CLUSTER and visualized using TREEVIEW.

Generation of *flagellin induced receptor kinase promoter-luciferase* plants. The firefly luciferase coding sequence was removed from pGL4-11 (Promega; GenBank accession AF234298) by Fse1 digestion, T4 DNA polymerase treatment followed by Kpn1 digestion. This fragment was ligated into pCambia1302 digested with Kpn1 and Pml1 to generate pCAMBIA-LUC2P. Amplification of the *FRK1* (At2g19190) promoter with *FRK1* Kpn1 5′-TT***GGTACC***GGACAACCACGGAAGTTATTAGC-3′ and FRK1 Nco1 5′-GACCCG***GGTACC***GAGAAGTTTGG-3′ primers generated a 2,152 bp fragment that was digested with Kpn1 and Nco1 and ligated into the complementary sites of the pCAMBIA-LUC2P derivative. Sequence validated constructs were transformed into *Agrobacterium. tumefaciens* (GV3101) used to transform *Arabidopsis thaliana* ecotype Col-0 by the floral dip method. Transgenic lines were selected on gentamycin and homozygous lines isolated.

Effector import into chloroplasts. Effector N-termini (about 150 aa), fused to GFP, were radiolabelled by *in vitro* expression (TNT T7 reticulocyte lysate kit, Promega). Import into isolated pea chloroplasts[35] equivalent to 20 µg of chlorophyll was allowed for 1 h at 30 °C. Subsequently, chloroplasts were re-purified and half of the reaction was incubated with 2 µg thermolysin for 20 min on ice to digest non-imported proteins. Reaction products were separated by SDS-PAGE and visualized on X-ray films.

Received 30 October 2014; accepted 24 April 2015; published online XX XX 2015

References

1. Bohm, H., Albert, I., Fan, L., Reinhard, A. & Nurnberger, T. Immune receptor complexes at the plant cell surface. *Curr. Opin. Plant Biol.* **20C,** 47–54 (2014).
2. Macho, A. P. & Zipfel, C. Plant PRRs and the activation of innate immune signaling. *Mol. Cell* **54,** 263–272 (2014).
3. Shapiguzov, A., Vainonen, J. P., Wrzaczek, M. & Kangasjarvi, J. ROS-talk – how the apoplast, the chloroplast, and the nucleus get the message through. *Front. Plant Sci.* **3,** 292 (2012).
4. Galvez-Valdivieso, G. & Mullineaux, P. M. The role of reactive oxygen species in signalling from chloroplasts to the nucleus. *Physiol. Planta* **138,** 430–439 (2010).
5. Robert-Seilaniantz, A., Grant, M. & Jones, J. D. Hormone crosstalk in plant disease and defense: more than just jasmonate-salicylate antagonism. *Annu. Rev. Phytopathol.* **49,** 317–343 (2011).
6. Trotta, A., Rahikainen, M., Konert, G., Finazzi, G. & Kangasjarvi, S. Signalling crosstalk in light stress and immune reactions in plants. *Phil. Trans. R. Soc. B* **369,** 20130235 (2014).
7. Cunnac, S., Lindeberg, M. & Collmer, A. Pseudomonas syringae type III secretion system effectors: repertoires in search of functions. *Curr. Opin. Microbiol.* **12,** 53–60 (2009).
8. Truman, W., Zabala, M. D. T. & Grant, M. Type III effectors orchestrate a complex interplay between transcriptional networks to modify basal defense responses during pathogenesis and resistance. *Plant J.* **46,** 14–33 (2006).
9. Smyth, G. K., Michaud, J. & Scott, H. S. Use of within-array replicate spots for assessing differential expression in microarray experiments. *Bioinformatics* **21,** 2067–2075 (2005).
10. Zipfel, C. *et al.* Bacterial disease resistance in Arabidopsis through flagellin perception. *Nature* **428,** 764–767 (2004).
11. Windram, O. *et al.* Arabidopsis defense against Botrytis cinerea: chronology and regulation deciphered by high-resolution temporal transcriptomic analysis. *Plant Cell* **24,** 3530–3557 (2012).
12. Grant, M. *et al.* The RPM1 plant disease resistance gene facilitates a rapid and sustained increase in cytosolic calcium that is necessary for the oxidative burst and hypersensitive cell death. *Plant J.* **23,** 441–450 (2000).
13. Baker, N. R. Chlorophyll fluorescence: a probe of photosynthesis in vivo. *Annu. Rev. Plant Biol.* **59,** 89–113 (2008).
14. Muller, P., Li, X. P. & Niyogi, K. K. Non-photochemical quenching. A response to excess light energy. *Plant Physiol.* **125,** 1558–1566 (2001).
15. Zheng, X. Y. *et al.* Coronatine promotes Pseudomonas syringae virulence in plants by activating a signaling cascade that inhibits salicylic acid accumulation. *Cell Host Microbe* **11,** 587–596 (2012).
16. Gohre, V., Jones, A. M., Sklenar, J., Robatzek, S. & Weber, A. P. Molecular crosstalk between PAMP-triggered immunity and photosynthesis. *Mol. Plant Microbe Interact.* **25,** 1083–1092 (2012).
17. de Torres Zabala, M., Bennett, M. H., Truman, W. H. & Grant, M. R. Antagonism between salicylic and abscisic acid reflects early host-pathogen conflict and moulds plant defence responses. *Plant J* (2009). Q3
18. Debener, T., Lehnackers, H., Arnold, M. & Dangl, J. L. Identification and molecular mapping of a single Arabidopsis thaliana locus determining resistance to a phytopathogenic Pseudomonas syringae isolate. *Plant J.* **1,** 289–302 (1991).
19. Taylor, J. D., Conway, J., Roberts, S. J., Astley, D. & Vicente, J. G. Sources and origin of resistance to Xanthomonas campestris pv. campestris in brassica genomes. *Phytopathology* **92,** 105–111 (2002).
20. Kvitko, B. H. *et al.* Deletions in the repertoire of Pseudomonas syringae pv. tomato DC3000 type III secretion effector genes reveal functional overlap among effectors. *PLoS Pathogens* **5,** e1000388 (2009).
21. Cunnac, S. *et al.* Genetic disassembly and combinatorial reassembly identify a minimal functional repertoire of type III effectors in Pseudomonas syringae. *Proc. Natl Acad. Sci. USA* **108,** 2975–2980 (2011).
22. Gomez-Gomez, L. & Boller, T. Flagellin perception: a paradigm for innate immunity. *Trends Plant Sci.* **7,** 251–256 (2002).
23. Kunze, G. *et al.* The N terminus of bacterial elongation factor Tu elicits innate immunity in Arabidopsis plants. *Plant Cell* **16,** 3496–3507 (2004).
24. Wiermer, M., Feys, B. J. & Parker, J. E. Plant immunity: the EDS1 regulatory node. *Curr. Opin. Plant Biol.* **8,** 383–389 (2005).
25. de Torres-Zabala, M. *et al.* Pseudomonas syringae pv. tomato hijacks the Arabidopsis abscisic acid signalling pathway to cause disease. *EMBO J.* **26,** 1434–1443 (2007).
26. Rubio, S. *et al.* Triple loss of function of protein phosphatases type 2C leads to partial constitutive response to endogenous abscisic acid. *Plant Physiol.* **150,** 1345–1355 (2009).
27. Asai, T. *et al.* MAP kinase signalling cascade in Arabidopsis innate immunity. *Nature* **415,** 977–983 (2002).
28. Figueiredo, J. F. *et al.* Agrobacterium-mediated transient expression in citrus leaves: a rapid tool for gene expression and functional gene assay. *Plant Cell Rep.* **30,** 1339–1345 (2011).
29. Jelenska, J. *et al.* A J domain virulence effector of Pseudomonas syringae remodels host chloroplasts and suppresses defenses. *Curr. Biol.* **17,** 499–508 (2007).
30. Li, G. *et al.* Distinct Pseudomonas type-III effectors use a cleavable transit peptide to target chloroplasts. *Plant J.* **77,** 310–321 (2014).
31. Rodriguez-Herva, J. J. *et al.* A bacterial cysteine protease effector protein interferes with photosynthesis to suppress plant innate immune responses. *Cell. Microbiol.* **14,** 669–681 (2012).
32. Jelenska, J., van Hal, J. A. & Greenberg, J. T. Pseudomonas syringae hijacks plant stress chaperone machinery for virulence. *Proc. Natl Acad. Sci. USA* **107,** 13177–13182 (2010).
33. Emanuelsson, O., Brunak, S., von Heijne, G. & Nielsen, H. Locating proteins in the cell using TargetP, SignalP and related tools. *Nature Protocols* **2,** 953–971 (2007).
34. Mukhtar, M. S. *et al.* Independently evolved virulence effectors converge onto hubs in a plant immune system network. *Science* **333,** 596–601 (2011).
35. Waegemann, K. & Soll, J. Characterization of the protein import apparatus in isolated outer envelopes of chloroplasts. *Plant J.* **1,** 149–158 (1991).
36. Macho, A. P. *et al.* Genetic analysis of the individual contribution to virulence of the type III effector inventory of Pseudomonas syringae pv. phaseolicola. *PLoS One* **7,** e35871 (2012).
37. Fu, Z. Q. *et al.* A type III effector ADP-ribosylates RNA-binding proteins and quells plant immunity. *Nature* **447,** 284–288 (2007).
38. Baba, K., Nakano, T., Yamagishi, K. & Yoshida, S. Involvement of a nuclear-encoded basic helix-loop-helix protein in transcription of the light-responsive promoter of psbD. *Plant Physiol.* **125,** 595–603 (2001).
39. Shi, L. X. & Schroder, W. P. The low molecular mass subunits of the photosynthetic supracomplex, photosystem II. *Biochim. Biophys. Acta* **1608,** 75–96 (2004).
40. Ikeuchi, M. *et al.* Cloning of the psbK gene from Synechocystis sp. PCC 6803 and characterization of photosystem II in mutants lacking PSII-K. *J. Biol. Chem.* **266,** 11111–11115 (1991).
41. Wessling, R. *et al.* Convergent targeting of a common host protein-network by pathogen effectors from three kingdoms of life. *Cell Host Microbe* **16,** 364–375 (2014).
42. Torres, M. A., Jones, J. D. & Dangl, J. L. Reactive oxygen species signaling in response to pathogens. *Plant Physiol.* **141,** 373–378 (2006).
43. Mitchell, K., Brown, I., Knox, P. & Mansfield, J. The role of cell wall-based defences in the early restriction of non-pathogenic hrp mutant bacteria in Arabidopsis. *Phytochemistry* (2014). Q4
44. Hempel, S. L., Buettner, G. R., O'Malley, Y. Q., Wessels, D. A. & Flaherty, D. M. Dihydrofluorescein diacetate is superior for detecting intracellular oxidants: comparison with 2′,7′-dichlorodihydrofluorescein diacetate, 5(and 6)-carboxy-2′,7′-dichlorodihydrofluorescein diacetate, and dihydrorhodamine 123. *Free Rad, Biol. Med.* **27,** 146–159 (1999).
45. Halliwell, B. & Whiteman, M. Measuring reactive species and oxidative damage in vivo and in cell culture: how should you do it and what do the results mean? *Brit. J. Pharmacol.* **142,** 231–255 (2004).
46. Mubarakshina, M. M. *et al.* Production and diffusion of chloroplastic H2O2 and its implication to signalling. *J. Exp. Bot.* **61,** 3577–3587 (2010).

47. Flors, C. *et al.* Imaging the production of singlet oxygen in vivo using a new fluorescent sensor, Singlet Oxygen Sensor Green. *J. Exp. Bot.* **57,** 1725–1734 (2006).
48. Krieger-Liszkay, A. Singlet oxygen production in photosynthesis. *J. Exp. Botany* **56,** 337–346 (2005).
49. Lee, K. P., Kim, C., Landgraf, F. & Apel, K. EXECUTER1- and EXECUTER2-dependent transfer of stress-related signals from the plastid to the nucleus of Arabidopsis thaliana. *Proc. Natl Acad. Sci. USA* **104,** 10270–10275 (2007).
50. Larkin, R. M. Influence of plastids on light signalling and development. *Phil. Trans. R. Soc. B* **369,** 20130232 (2014).
51. Allemeersch, J. *et al.* Benchmarking the CATMA microarray. A novel tool for Arabidopsis transcriptome analysis. *Plant Physiol.* **137,** 588–601 (2005).
52. Breeze, E. *et al.* High-resolution temporal profiling of transcripts during Arabidopsis leaf senescence reveals a distinct chronology of processes and regulation. *Plant Cell* **23,** 873–894 (2011).
53. Sharkey, T. D., Bernacchi, C. J., Farquhar, G. D. & Singsaas, E. L. Fitting photosynthetic carbon dioxide response curves for C(3) leaves. *Plant Cell Environ.* **30,** 1035–1040 (2007).
54. Littlejohn, G. R., Gouveia, J. D., Edner, C., Smirnoff, N. & Love, J. Perfluorodecalin enhances in vivo confocal microscopy resolution of Arabidopsis thaliana mesophyll. *New Phytol.* **186,** 1018–1025 (2010).

Acknowledgements

This work was funded by BBSRC grants BB/E010334/1 to M.G. and BB/F005903/1 to M.G. and N.S. M.T. and D.L. thank Ralph Bock and the Max Planck Society (MPG) for their support. We are indebted to members of the PRESTA consortium for their efforts in generating the microarray data. We thank Jean Greenberg for the Pma4326 *hopI1* strain and Emilia Lopez-Solanilla for the HopN1 derivatives. We are indebted to Krzysztof Polanski for generating the images for Fig. 1b.

Author contributions

M.G., M.d.T., J.M., M.T. and N.S. conceived the experiments, M.T., D.L., L.D. and B.B. undertook the chloroplast localization and effector predictions, S.J., T.B. and D.S. the bioinformatics, T.L., N.S. the photosynthesis experiments, G.L. the microscopy and M.d.T. and W.T. contributed to the remainder of the experimental work. M.d.T., M.G., N.S., J.M. and M.T. wrote the manuscript.

Additional information

Supplementary information is available online. Reprints and permissions information is available online at www.nature.com/reprints. Correspondence and requests for materials should be addressed to M.G.

Competing interests

The authors declare no competing financial interests.

Journal: NPLANTS

Article ID: nplants.2014.74

Article Title: Chloroplasts play a central role in plant defence and are targeted by pathogen effectors

Author(s): Marta de Torres-Zabala *et al.*

Query no.	Queries	Response
Q1	Please check the use of italics for variables throughout and correct if necessary.	
Q2	Please check that all highlighted text is correct and amend if necessary.	
Q3	Please provide volume and page numbers for reference 17.	
Q4	Please provide volume and page numbers for reference 43.	
Q5	Please check Additional information section is correct	